Journal of Magnetism and Magnetic Materials 354 (2014) 216–221

Contents lists available at ScienceDirect

Journal of Magnetism and Magnetic Materials

journal homepage: www.elsevier.com/locate/jmmm

Thermoelectric properties, electronic structure and optoelectronic properties of anisotropic $Ba_2Tl_2CuO_6$ single crystal from DFT approach

A.H. Reshak [a,b], Saleem Ayaz Khan [a,*]

[a] New Technologies - Research Center, University of West, Bohemia, Univerzitni 8, 30614 Pilsen, Czech Republic
[b] Center of Excellence Geopolymer and Green Technology, School of Material Engineering, University Malaysia Perlis, 01007 Kangar, Perlis, Malaysia

ARTICLE INFO

Article history:
Received 26 August 2013
Received in revised form
2 November 2013
Available online 13 November 2013

Keywords:
Superconductor
Fermi surface
Optical property
Seebeck coefficient

ABSTRACT

First principle calculation was performed for the electronic structure, electronic charge density, Fermi surface, optical and thermoelectric properties of $Ba_2Tl_2CuO_6$ compound. From the electronic band structure the two overlapping bands and the density of state at Fermi level (29.2 states/Ryd-cell) confirms the superconducting behavior. Colors of the Fermi surface elucidate speed of electrons and strength of the superconductivity as well. The bonding nature was investigated using the calculated charge density contour plot, it shows mixed ionic-covalent nature of Cu–O and Tl–O while Ba–O shows dominant ionic nature with small covalency. The optical properties were calculated and discussed in details. The calculated uniaxial anisotropy value (0.7913) clarifies a considerable anisotropy between two dominant tensor components of dielectric function. Moreover the evaluation of Seebeck coefficient and thermal conductivity conform that the compound is much suitable for thermoelectric applications.

1. Introduction

In recent years a number of interesting studies has been performed on superconductivity because of its momentous applications. The superconductor's digital electronics (SDE) give a distinctive arrangement of ultra-low-power and fast switching consumption [1–3]. Gündogmus et al. [4] calculated the mechanical, physical and magnetic properties of the Yb-doped $Bi_2Sr_2Ca_1Cu_2O_y$ textured superconductor and discussed the variation in superconductivity with different doping concentration of Yb. A distinct variety of superconductors were discovered by substituting rare earth in Ba–Cu–O system for example Y–Ba–Cu–O or La–Ba–Cu–O [5,6]. The concept of substitution were used generally in X_{111}–Y_{11}–Cu–O scheme where X_{111} = rare earth element and Y_{11} = Ca, Sr, Pb which led to the discovery of a new class of superconductors. Claughton and Lambert [7] built up a general frame to illustrate the thermoelectric effects in phase-coherent superconducting structures. Superconductors exhibit admirable electrical conductivity and poor thermal conductivity which make it suitable for thermoelectric properties [8]. For thermoelectricity, the principal role is played by electron–phonon anharmonicities [9].

Hamann et al. [10] calculated the electronic structure of $Ba_2Tl_2CuO_6$ by local density approximation with the use of the relativistic version of linear augmented plane wave method which is not accurate as the full potential method. They discussed the electronic band structure, density of state and electronic charge density of $Ba_2Tl_2CuO_6$ compound, but still there are some deficiencies. In the present work we deal with the electronic band structure, density of state, electronic charge density, optical properties and thermoelectric properties of the investigated compound in a more fascinating way which provides complete information about the nature of the material by using the full potential linear augmented plane wave (FPLAPW) method which has been proven to be one of the most accurate methods for the computation of electronic, thermoelectric and optical properties of solid within density functional theory (DFT) [11,12].

2. Crystal structure and method of calculation

The crystal structure of $Ba_2Tl_2CuO_6$ is stable in tetragonal phase having space group (I4/mm). The crystallographic data of the reported compound is taken from Ref. [10]. The all electron full potential linear augmented plane wave (FPLAPW) method within the frame work of WIEN2K code [13] was used for calculating the electronic structure, density of state, Fermi surface, optical properties and thermoelectric properties. The exchange correlation energy is solved by Ceperley–Alder (CA) local density approximation (CA-LDA) [14], Perdew–Burke–Ernzerhof generalized gradient approximation (PBE-GGA) [15], and Engle Vasko generalized gradient approximation (EV-GGA) [16] schemes. For convergence of energy eigenvalues the wave function in the interstitial regions were expended in plane waves with cutoff $R_{MT}K_{max} = 7.0$. Where R_{MT} stands for muffin-tin (MT) sphere radius and K_{max} represents the magnitude of largest K

* Corresponding author.
E-mail address: sayaz_usb@yahoo.com (S.A. Khan).

0304-8853/$ - see front matter © 2013 Elsevier B.V. All rights reserved.
http://dx.doi.org/10.1016/j.jmmm.2013.11.014

vector in plane wave expansion. A mish of $9\times9\times9$ **k** points in Brillouin zone (BZ) were used. The muffin-tin (MT) sphere radii (R_{MT}) were selected as 1.92 a.u. for Cu atom, 2.5 a.u. for Ba, 1.85 a.u. for Tl and 1.7 a.u. for O atom. Inside atomic sphere the wave function was expended up to $l_{max}=10$ where as the Fourier expansion of the charge density was up to $G_{max}=12(\text{a.u.})^{-1}$. We have optimized the structure by minimization of forces acting on the atoms. The convergence of the self-consistent calculations were achieved when the difference in total energy of the crystal did not exceed 10^{-5} Ryd for successive steps. The self-consistencies were obtained by 75 **k** points in irreducible Brillouin zone (IBZ), initiated from 500 **k** points in the BZ. Fig. 1

3. Results and discussion

3.1. Band structure and density of state

The importance of electronic band structure cannot be ignored because of direct influence over the physical properties of many compounds [17,18]. The high symmetry points were selected to calculate electronic band structure of $Ba_2Tl_2CuO_3$ by three schemes LDA-CA, GGA-PBE and EV-GGA as shown in Fig. 2. The calculated band structures elucidate that band # 67 and 68 cuts the Fermi level resulting in a metallic nature of the investigated compound. The three schemes show almost same results around Fermi level except that EV-GGA shift the upper conduction bands towards higher energy as compared to LDA-CA and GGA-PBE. One can also see this effect in total density of state (TDOS) as illustrated in Fig. 3a. This is mainly due to the fact that EV-GGA is sufficiently flexible and able to reproduce the exchange–correlation energy and its charge derivative accurately. Our previous experience [19] also support EV-GGA for close agreement with experimental data therefore this scheme was preferred for further details. Fig. 3a–g represents the calculated total and partial density of states.

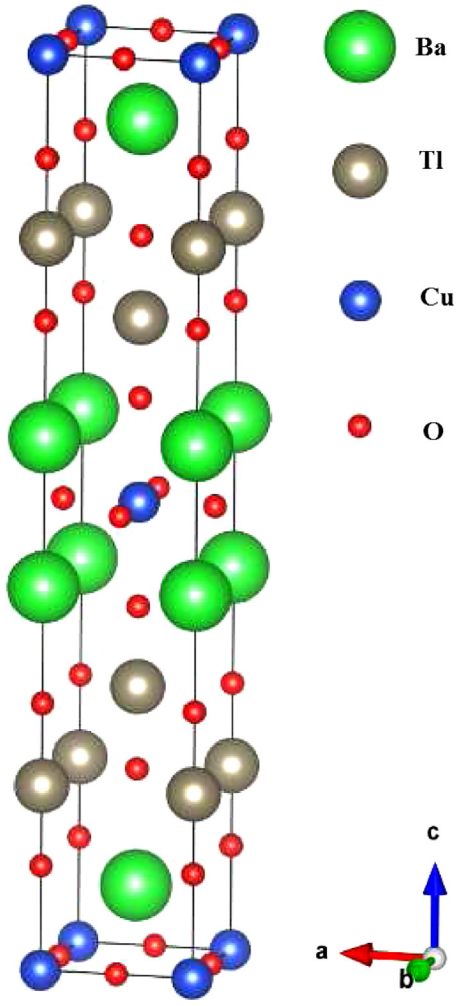

Fig. 1. Optimize unit cell of $Ba_2Tl_2CuO_6$ superconductor.

The PDOS shown in Fig. 3b–g visualizes that in energy range from −15.0 eV to −18.0 eV, the O-s, Cu-p/d, Ba-s/p and Tl-p/f states contribute to form the core bands. The O-s state is foremost (2.2 states/eV) while the contribution of the other states is small. In the energy range between −11.5 eV and −12.7 eV the bands are formed mainly from Tl-d (18.0 states/eV) and Ba-p (8.0 states/eV) states with negligible contribution of Cu-p, Ba-s, O-s/p and Tl-s states. The Cu-d and O-p states are dominant in energy range between −7.5 eV and −1.0 eV while the other states (Cu-s/p, Ba-s/p/d and Tl-s/p) contribute negligibly. The bands around the Fermi level (from −1.0 to 1.0 eV) are fashioned by Cu-s/p/d, Ba-p, O-p and Tl-s states. Cu-d state is more responsible to form bands in this region. From 4.5 to 12.0 eV the Ba-d state shows dominancy while Cu-s/p, Ba-s and Tl-s/p/f states take part in band formation with small values.

3.2. Fermi surface

The density of state at Fermi level $N(E_F)$ for $Ba_2Tl_2CuO_6$ can be obtained from the overlapping of band # 66 and band # 67. These bands mainly originated from Cu-d and O-p states with small contribution of Cu-s/p, Ba-s/p/d and Tl-s/p/f states, which are responsible for the superconducting state of the material. The electronic specific heat (γ) which is the function of density of state can be determined by using the expression given in Ref. [20]:

$$\gamma=\tfrac{1}{3}\pi^2N(E_F)k_B^2 \tag{1}$$

where k_B is Boltzman constant. The calculated value of $N(E_F)$ and γ are 29.2 states/Ryd-cell and 5.06 mJ/mol K^2. Fig. 4a–c shows the shape of Fermi surface formed by band # 66 and 67 individually and the final shape of Fermi surface. We should emphasize that white regions in Fig. 4 represent the hole concentration while the color sheet shows the presence of electrons. The colors of Fermi surface (red, yellow, cerulean and blue) represent the variation in the electron velocities which is directly related to the superconductivity of the material.

3.3. Electronic charge density

The accurate bond nature of the material can be explained on the basis of electronic charge density contour plot [21,22]. We have calculated the distribution of charge density in the (0 1 0) crystallographic plane in order to visualize the chemical bonding nature of the constituent in $Ba_2Tl_2CuO_3$ single crystal as shown in Fig. 5. As it is clear from the scale the red color shows zero charge density regions while blue one exposes maximum charge intensity. The Cu atoms share its valence electrons with O atoms forming mixed ionic-covalent bond. The blue region around O atoms shows maximum charge density region and this is due to highest electro-negativity value (3.44) as compared to Cu atom (1.90) and same is the case for Tl–O. Moreover the O atom shares its charge with four Ba atoms on each face of the unit cell in the same manner forming dominant ionic bond having less part of covalency. This is due to the small electro-negativity value of Ba (0.890) in comparison to the O atom.

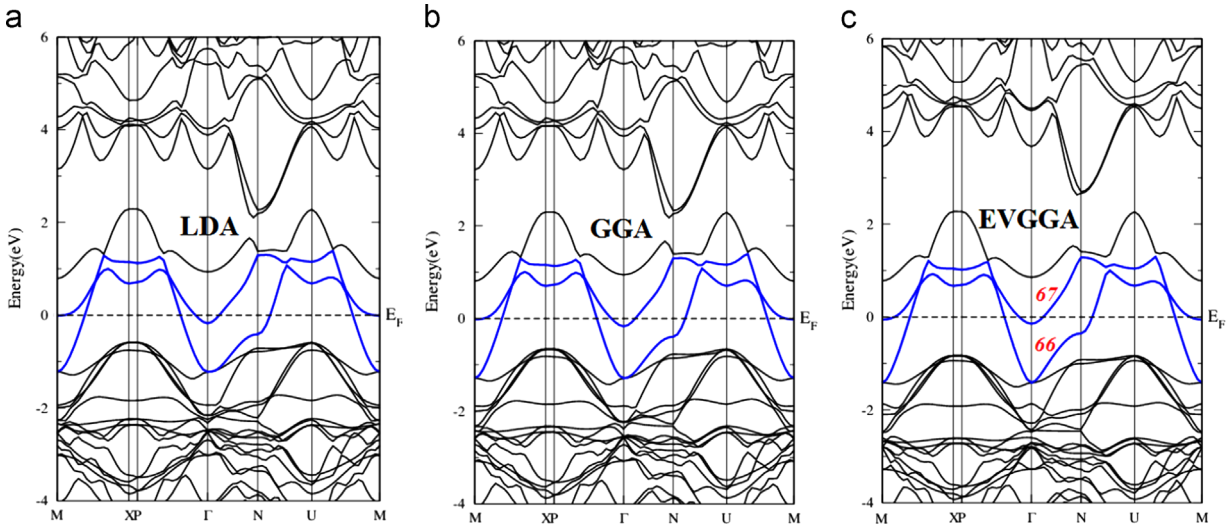

Fig. 2. Calculated band structure of $Ba_2Tl_2CuO_6$ semiconductor by (a) LDA, (b) GGA-PBE, and (c) EVGGA.

3.4. Optical and thermoelectric properties

We have used our calculated band structure to obtain the imaginary part of the frequency dependent dielectric function. The dispersion of dielectric function includes intra- and inter-band transitions. The intra-band transitions belong to the same band and show significant effect in case of metals while the inter-band (band to band) transitions are further divided into direct and indirect band transitions. The correct energy eigenvalues and electron wave functions are required for calculating the dispersion dielectric function $\varepsilon(\omega)$ [23–25]. The single crystal of $Ba_2Tl_2CuO_3$ has tetragonal symmetry which permit only two principal diagonal non-zero second order dielectric tensor components $\varepsilon^{xx}(\omega)=\varepsilon^{\perp}(\omega)$ and $\varepsilon^{zz}(\omega)=\varepsilon^{II}(\omega)$ along a and c crystallographic axes. These dielectric tensor components are sufficient for the full explanation of linear optical susceptibilities. One can obtain the required components by using the expression given in Ref. [26]:

$$\varepsilon_2^{ij}=\frac{4\pi^2e^2}{Vm^2\omega^2}\times\sum_{nn'\sigma}\langle kn\sigma|p_i|kn'\sigma\rangle\langle kn'\sigma|p_j|kn\sigma\rangle\times f_{kn}(1-f_{kn'})\delta(E_{kn'}-E_{kn}-\hbar\omega) \quad (2)$$

where e and m symbolize both charge and mass of electron, ω and V stands for electromagnetic radiation striking the crystal and unit cell volume, the bracket notation $|kn\sigma\rangle$ stands for crystal wave function with crystal momentum k, and σ spin symbolizes the eigenvalueE_{kn} corresponding to the momentum operator p_j. The Fermi distribution function (f_{kn}) makes sure the counting of transition from occupied to unoccupied and $\delta(E_{kn'}-E_{kn}-\hbar\omega)$ shows the form for total energy conservation. The allowed electric-dipole transitions between occupied and unoccupied states can be seen in the spectral peaks of absorptive part $\varepsilon_2(\omega)$ which can be identified from the magnitude of the optical matrix elements. As $Ba_2Tl_2CuO_3$ compound is metallic, we have to include the Drude term following the expression given in Ref. [27]:

$$\varepsilon_2^{\perp}(\omega)=\varepsilon_{2intra}^{\perp}(\omega)+\varepsilon_{2inter}^{\perp}(\omega) \quad (3)$$

where

$$\varepsilon_{2intra}^{\perp}(\omega)=\frac{\omega_p^{\perp 2}\tau}{\omega(1+\omega^2\tau^2)} \quad (4)$$

in the expression τ is the relaxation time and $\omega_p^{\perp}$ is anisotropic plasma frequency given as [28]:

$$\omega_p^{\perp 2}=\frac{8\pi}{3}\sum_{kn}\nu_{kn}^{\perp 2}\delta(\varepsilon_{kn}) \quad (5)$$

$\nu_{kn}^{\perp}$ represents velocity of electron in the Bessel plane and ε_{kn} shows the difference between $E_n(k)$ and E_F. In the same way one can write the expressions of the parallel components of the dielectric tensors.

Fig. 6a and b, represents the calculated $\varepsilon_2^{\perp}(\omega)$ and $\varepsilon_2^{II}(\omega)$ spectra with and without Drude terms, respectively. The effect of the Drude term is foremost on low energy level (less than 1.0 eV) [29]. The structures of $\varepsilon_2(\omega)$ at the energies greater than 1.0 eV are due to inter-band transitions as shown in Fig. 6b. The first peak (greater than 1.0 eV) shows transition of electrons from Cu-d and O-p state to Tl-s/d and Cu-p state. The next peak shows electron transition from Cu-s/p/d and O-p state to Cu-s, Tl-p and Ba-d state. The peaks around 8.3 eV and 9.1 eV are due the probability of electron transition from Cu-s/p/d and O-p states to Cu-s, Ba-s and Tl-p states. Similarly the next peak around 10.7 eV is initiated from electron transition from Cu-s/d, Ba-s, O-p states to Cu-s/p, Ba-s/d, Tl-p states. The tail of the spectra in the energy range from 11 eV to 14 eV is fashioned by electron transition probably from Cu-s/d, Tl-s and O-p states to Cu-s, Ba-s and Tl-p/f states. There exists a considerable anisotropy between $\varepsilon_2^{\perp}(\omega)$ and $\varepsilon_2^{II}(\omega)$ for the whole range.

Using the imaginary part of the dielectric function we have obtained the real part of the dielectric function using the Kramers–Kronig relation [30]:

$$\varepsilon_1(\omega)=1+\frac{2}{\pi}P\int_0^{\infty}\frac{\omega'\varepsilon_2(\omega')}{\omega'^2-\omega^2}d\omega'$$

where P stands for the principal value of integral. Fig. 6c shows $\varepsilon_1^{\perp}(\omega)$ and $\varepsilon_1^{II}(\omega)$ including the Drude term while Fig. 6d shows the dispersion of real part without Drude term. The uniaxial anisotropy was calculated to be 0.7913, using expression $\delta\varepsilon=[(\varepsilon_0^{II}-\varepsilon_0^{\perp})/\varepsilon_0^{tot}]$ taken from Ref. [31], which elucidated that there is a considerable anisotropy between the dielectric tensor components of the real part.

The calculated tensor components of the refractive indices $n^{\perp}(\omega)$ and $n^{II}(\omega)$ confirm the anisotropic behavior. We should emphasize that $n^{II}(\omega)$ falls below unity at around 6.4 eV which changes the behavior of the material from linear to nonlinear. The extension coefficient plays a very important role in metals. It shows absorption

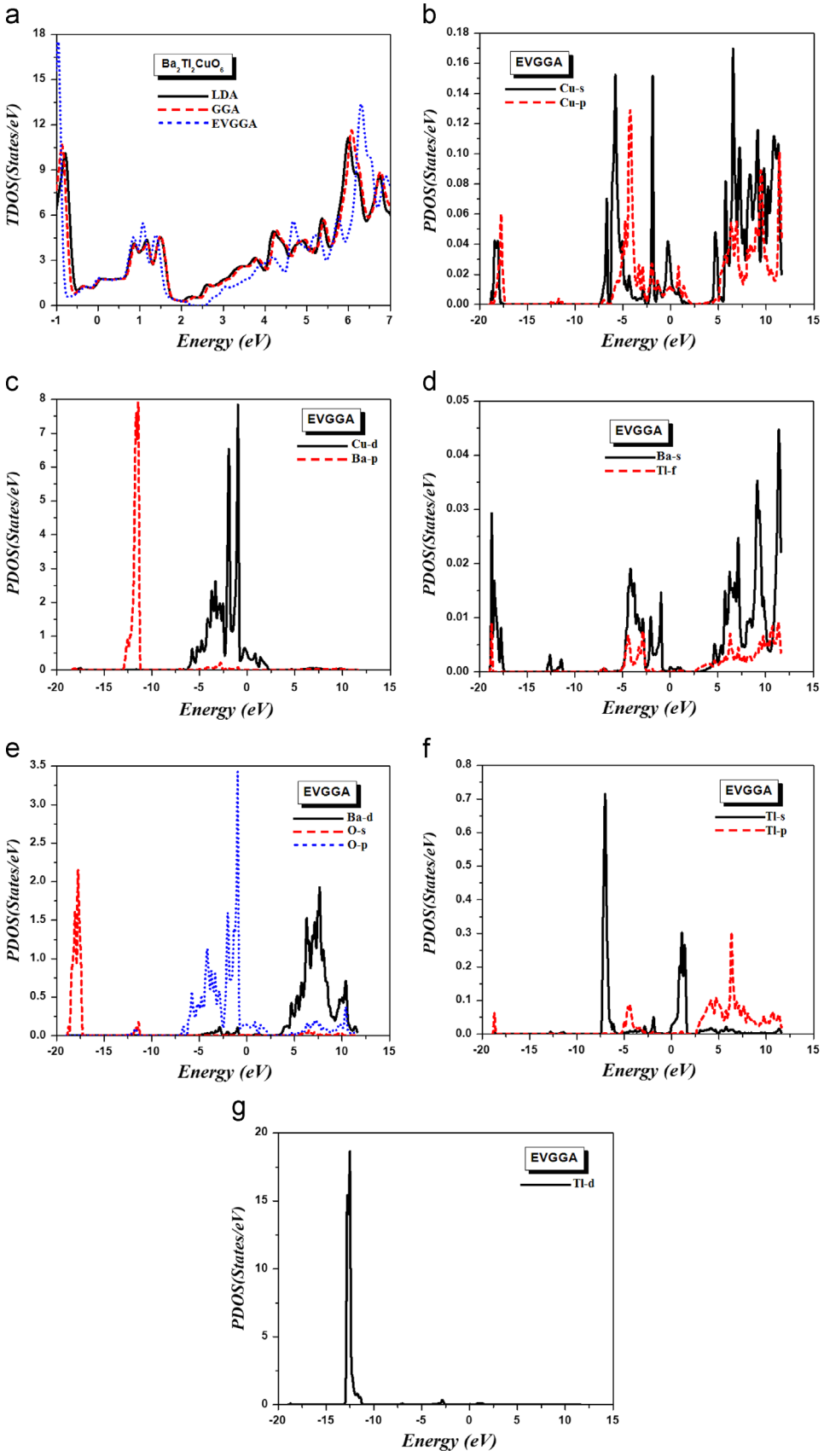

Fig. 3. Calculated total and partial densities of states (states/eV unit cell).

of energy on the skin (layer of charge on metal surface) of the material. $k^{II}(\omega)$ is dominant from 0.0 to 3.7 eV and from 4.3 to 9.0 eV whereas the rest of the range shows dominancy in $k^{\perp}(\omega)$ components. The maximum skin absorption by $k^{II}(\omega)$ is shown around 6.2 eV. The spectra of absorption coefficient show that $I^{II}(\omega)$ has maximum value around 6.2 eV while $I^{\perp}(\omega)$ gave maximum peak around 11.0 eV.

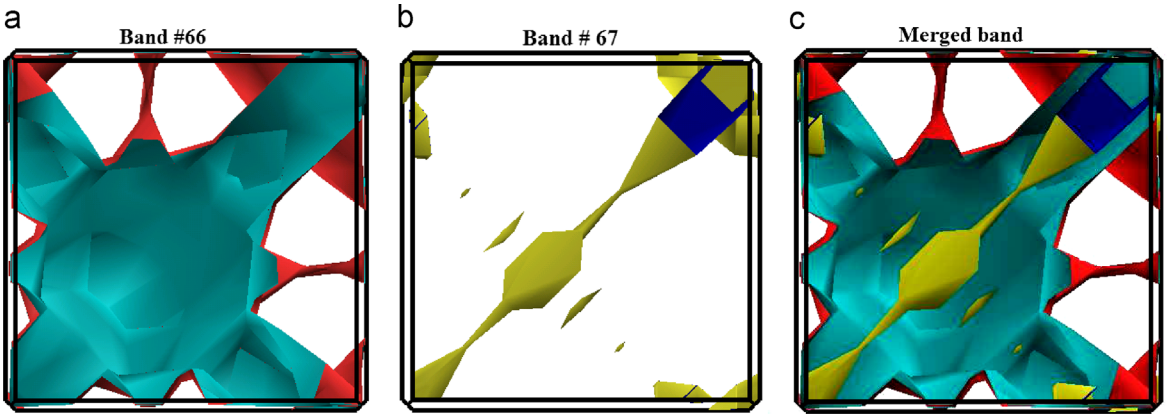

Fig. 4. Calculated Fermi surface of (a) band # 66, (b) band # 67, and (c) merged band.

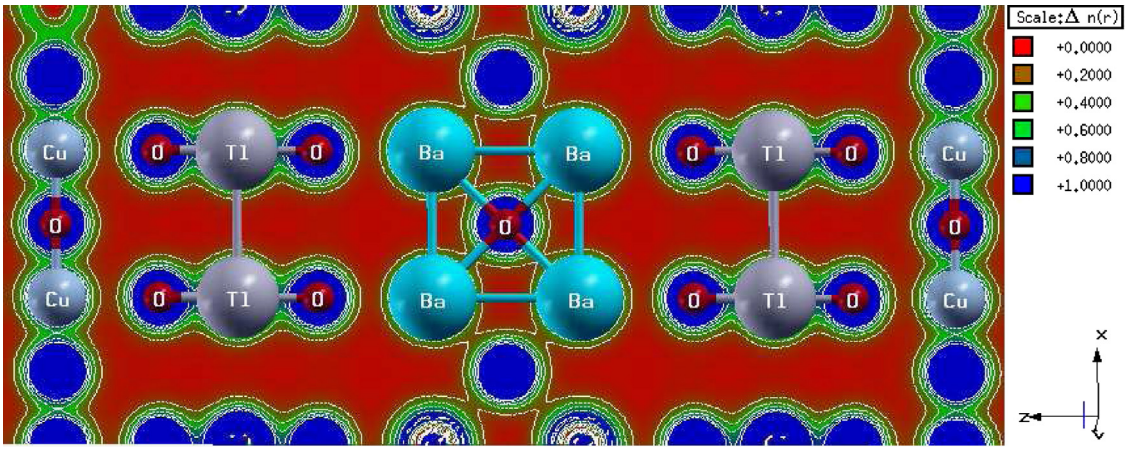

Fig. 5. Electronic charge density contour of $Ba_2Tl_2CuO_6$ in (010) plane.

The reflectivity is more suitable observable for metal-superconductors. It is commonly used in determining conductivity at near optical frequencies [32]. The reflectivity spectra of $Ba_2Tl_2CuO_3$ show that $R^{II}(\omega)$ plays leading role towards higher reflectivity value while the $R^{\perp}(\omega)$ component shows less reflectivity as compared to the $R^{II}(\omega)$. The reflectivity spectra of $R^{II}(\omega)$ elucidate the maximum value (60% and 65%) around 6.2 eV and 13.4 eV. The calculated imaginary and real parts of optical conductivity assign the response of the material to electromagnetic waves. The optical conductivity $\sigma(\omega)$ is correlated to the dielectric function $\varepsilon(\omega)=1+4\pi i\sigma(\omega)/\omega$ [33]. The Re $\sigma^{II}(\omega)$ spectra of $Ba_2Tl_2CuO_3$ reach the maximum photocurrent at around 6.0 eV.

The Seebeck coefficient and thermal conductivity were calculated by BoltzTraP program based semi-classical transport theory [34]. The sign and magnitude of the Seebeck coefficient are related to an asymmetry of the electron distribution around the Fermi level [35]. $S^{\perp}$ and S^{II} represent the perpendicular and parallel dielectric tensor components of the Seebeck coefficient which shows considerable anisotropy between the two components. S^{II} is more responsible for thermoelectric properties. Its first peak around 150 K shows the concentration of the hole. Further increasing the temperature results decrease in S^{II} and shows minimum value ($-160\ \mu V/K$) at high temperature while $S^{\perp}$ assigns the electron concentration with insignificant value of the Seebeck coefficient ($-20\ \mu V/K$) as compared to S^{II}. Thermal conductivity is also very important for calculation of thermoelectric properties leading to a significant increase of thermoelectric figure-of-merit (ZT) by expression $ZT=S^2T\sigma/(k_{el}+k_{ph})$ [36]. Both $k^{\perp}/\tau$ and k^{II}/τ show considerable anisotropy. k^{II}/τ starts from zero, increases linearly with small increment, and gives a value of 0.1×10^{15} W/mKs around 2000 K while the $k^{\perp}/\tau$ shows 0.45×10^{15} W/mKs at 100 K and increases linearly for higher value of temperature and assigns a maximum value of 6.75×10^{15} W/mKs around 2000 K.

4. Conclusions

We have calculated the electronic band structure, density of state, electronic charge density, Fermi surface, optical and thermoelectric properties of $Ba_2Tl_2CuO_6$ compound. The investigation of electronic band structure exposed that there exist two bands overlapped around Fermi level. The calculated density of state around Fermi level is about 29.2 states/Ryd-cell and electronic specific heat is found to be 5.06 mJ/mol K^2, visualize the superconducting behavior of the compound. The observed colors of the Fermi surface elucidate the speed of electrons and also strength of the superconductivity. The calculated charge density contour plot was evaluated in terms of electro-negativity difference which shows prevailing ionic nature of the bonds with small fraction of covalency for Ba–O while both Cu–O and Tl–O shows mixed ionic-covalent nature. Further the complex part of dielectric tensor components was calculated with and without Drude term. The Drude term represents the intra-band transition of electron below 1.0 eV while the spectral peaks in higher energy range (above 1.0 eV) show electron transition from the occupied bands (below

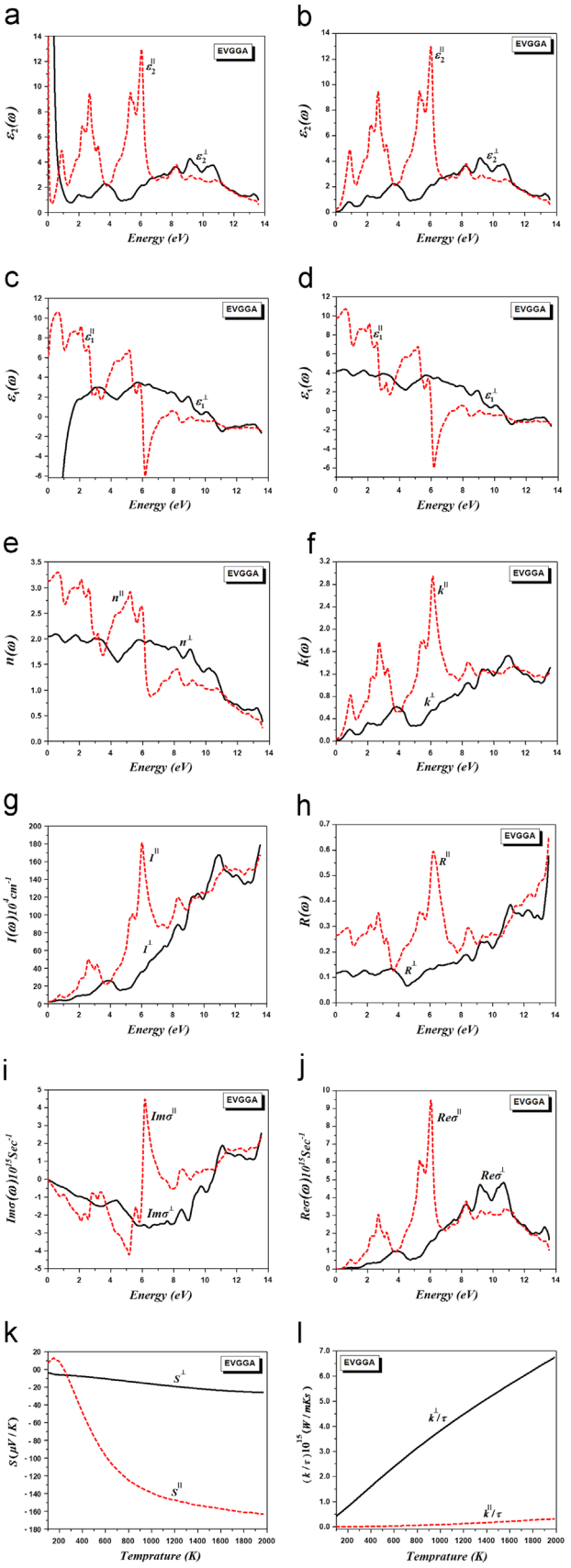

Fig. 6. (a) Calculated $\varepsilon_2(\omega)$ including Drude term, (b) calculated $\varepsilon_2(\omega)$ without Drude term, (c) calculated $\varepsilon_1(\omega)$ including Drude term, (d) calculated $\varepsilon_1(\omega)$ without Drude term, (e) calculated $n(\omega)$, (f) calculated $k(\omega)$, (g) calculated $I(\omega)$, (h) calculated $R(\omega)$, (i) calculated Im $\sigma(\omega)$, (j) calculated Re $\sigma(\omega)$, (k) calculated $S(\omega)$, and (l) calculated k/τ.

Fermi level) to highest unoccupied bands. The calculated uniaxial anisotropy confirms the considerable anisotropy between two principal tensor components of dielectric function. The other optical constants like refractive index $n(\omega)$, extension coefficient $k(\omega)$, absorption coefficient $I(\omega)$ and reflectivity $R(\omega)$ were calculated and discussed in detail. In additional we have calculated and discussed the Seebeck coefficient and thermal conductivity of $Ba_2Tl_2CuO_6$ compounds.

Acknowledgment

The result was developed within the CENTEM project, reg. no. CZ.1.05/2.1.00/03.0088, co-funded by the ERDF as part of the Ministry of Education, Youth and Sports OP RDI programme. School of Material Engineering, Malaysia University of Perlis, Malaysia.

References

[1] Q.Q. Ge, Z.R. Ye, M. Xu, Y. Zhang, J. Jiang, B.P. Xie, Y. Song, C.L. Zhang, Pengcheng Dai, D.L. Feng, Phys. Rev. X 3 (2013) 011020.
[2] A. Punitha, Sujin P. Jose, S. Mohan, J. Phys. Sci. 22 (2011) 33–49.
[3] T. Ortlepp, S.R. Whiteley, L. Zheng, X. Meng, T. Van Duzer, IEEE Transition Appl. Supercond. 23 (2013) 1400104.
[4] H. Gündogmus, B. Özçelik, B. Özkurt, A. Sotelo, M.A. Madre, J. Supercond. Nov. Magn. 26 (2013) 111–115.
[5] Z.Z. Sheng, A.M. Hermann, Nature 332 (1988) 55–58.
[6] Z.Z. Sheng, A.M. Hermann, Nature 332 (1988) 138–139.
[7] N.R. Claughton, C.J. Lambert, Phys. Rev. B 53 (1996) 6605–6612.
[8] A.F. Andreev, Sov. Phys. JETP 19 (1964) 1228.
[9] H. Kaddouri, S. Benet, S. Charar, M. Makowska-Janusik, J.C. Tedenac, I.V. Kityk, Phys. Rev. B 62 (2000) 17108–17116.
[10] D.R. Hamann, L.F. Mattheiss, Phys. Rev. B 38 (7) (1988) 5138–5141.
[11] S. Gao, Comput. Phys. Commun. 153 (2003) 190–198.
[12] K. Schwarz, J. Solid State Chem. 176 (2003) 319–328.
[13] P. Blaha, K. Schwarz, G. Madsen, D. Kvasnicka, J. Luitz, WIEN2K, An Augmented Plane Wave Plus Local Orbitals Program for Calculating Crystal properties, Vienna University of Technology, Austria, ISBN 3-9501031-1-2, 2001.
[14] D.M. Ceperley, B.I. Alder, Phys. Rev. Lett. 45 (1980) 566–569.
[15] J.P. Perdew, K. Burke, M. Ernzerhof, Phys. Rev. Lett. 77 (1996) 3865–3868.
[16] E. Engel, S.H. Voskov, Phys. Rev. B 47 (1993) 13164–13174.
[17] S.A. Khan, A.H. Reshak, Int. J. Electrochem. Sci. 8 (2013) 9459–9473.
[18] I. Khan, I. Ahmad, D. Zhang, H.A. Rahnamaye Aliabad, S.J. Asadabadi, J. Phys. Chem. Solids 74 (2013) 181–188.
[19] A.H. Reshak, S.A. Khan, H. Kamarudin, Jiri Bila, J. Alloys Compd. 582 (2014) 6–11.
[20] A.H. Reshak, H. Kamarudin, J. Alloys Compd. 509 (2011) 7861–7869.
[21] R. Hoffman, Rev. Mod. Phys. 60 (1988) 601–628.
[22] C.D. Gellatt, A.R. Willaims, V.L. Moruzzi, Phys. Rev. B 27 (1983) 2005–2013.
[23] B. Amin, R. Khenata, A. Bouhemadou, I. Ahmad, M. Maqbool, Physica B 407 (2012) 2588–2592.
[24] B. Amin, I. Ahmad, M. Maqbool, S. Goumri-Said, R. Ahmad, J. Appl. Phys. 109 (2011) 023109.
[25] A.H. Reshak, S.A. Khan, Comput. Mater. Sci. 78 (2013) 91–97.
[26] A. Delin, P. Ravindran, O. Eriksson, J.M. Wills, Int. J.Quantum Chem. 69 (1998) 349–358.
[27] F. Wooten, Optical Properties of Solids, Academic Press, New York, London, 1972.
[28] A.H. Reshak, S. Azam, J. Magn. Magn. Mater. 342 (2013) 80–86.
[29] A.H. Reshak, Z. Charifi, H. Baaziz, J. Solid State Chem. 183 (2010) 1290–1296.
[30] H. Tributsch, Z. Naturforsch. 32A (1977) 972.
[31] A.H. Reshak, Xuean Chen, S. Auluck, I.V. Kityk, J. Chem. Phys. 129 (2008) 204111–204118.
[32] R.T. Collins, Z. Schlesinger, F. Holtzberg, P. Chaudhari, C. Field, Phys. Rev. B (1989) 6571–6574.
[33] A.H. Reshak, H. Kamarudin, S. Auluck, J. Phys. Chem. B 116 (2012) 4677–4683.
[34] G.K.H. Madsen, D.J. Singh, Comput. Phys. Commun. 175 (2006) 67–71.
[35] J.M. Clemens, The Seebeck Coefficient, Lasance, Issue: November 2006, ⟨http://www.electronics-cooling.com/2006/11/the-seebeck-coefficient/⟩.
[36] D.J. Singh, Phys. Rev. B 81 (2010) 195217.